Nat. Hazards Earth Syst. Sci. Discuss., 3, 1137–1173, 2015
www.nat-hazards-earth-syst-sci-discuss.net/3/1137/2015/
doi:10.5194/nhessd-3-1137-2015


Natural Hazards and Earth System Sciences
Discussions



# Landslide susceptibility analysis ~~by means of~~ event-based ~~multi-temporal~~ landslide inventories

**C. M. Tseng**[1], **C. W. Lin**[2], **and W. D. Hsieh**[2]

[1]Department of Land Management and Development, Chang Jung Christian University, No. 1, Changda Road, Gueiren District, Tainan City, Taiwan
[2]Department of Earth Sciences, National Cheng Kung University, No. 1, University Road, Tainan City, Taiwan

Received: 24 December 2014 – Accepted: 19 January 2015 – Published: 5 February 2015

Correspondence to: C. M. Tseng (cmtseng@mail.cjcu.edu.tw)

Published by Copernicus Publications on behalf of the European Geosciences Union.



## Abstract

This study uses landslide inventory of ~~a~~ single typhoon ~~event~~ and Weight of Evidence (WOE) analysis to ~~establish~~ landslide susceptibility map of the Laonung River in southern Taiwan. Eight factors including lithology, elevation, slope, slope aspect, landform, Normalized Difference Vegetation Index (NDVI), distance to geological structure, and distance to stream are used to evaluate the susceptibility of landslide. Effect analysis and the assessment of grouped factors showed that lithology, slope, elevation, and NDVI are the dominant factors of landslides in the study area. Landslide susceptibility analysis with these four factors achieves over 90 % of the AUC (area under curve) of the success rate curve of all eight factors. Four landslide susceptibility models for four typhoons from 2007 to 2009 are established, and each model is cross validated. Results indicate that the best model should be constructed by using landslide inventory close to the landslide occurrence threshold and should reflect the most common spatial rainfall pattern in the study region for ideal simulation and validation results. The prediction accuracy of the best model in this study reached 90.2 %. The two highest susceptibility categories (very high and high levels) cover around 80 % of the total landslides in the study area.

## 1 Introduction

Landslides are a natural process that plays a key role in landscape evolution of mountainous and hilly environments. They also represent a serious hazard in many areas of the world (Brabb and Harrod, 1989; Cendrero and Dramis, 1996; Glade et al., 2005). In mountainous areas of Taiwan, where is located at convergent pale boundary and the annual rainfall is over 2500 mm, landslides and debris flows are major natural hazards that threaten human lives (Lin et al., 2013; Tseng et al., 2013). For example, Typhoon Morakot in August of 2009, with a maximum precipitation of over 2884 mm in 5 days, ~~induced~~ over 22 705 landslides, covering a total area of 274 km$^2$ in mountainous regions

throughout southern Taiwan, with some landslides covering areas of over 60 ha (Lin et al., 2011). One deep-seated landslide, the Hsiaolin landslide, covering an area of about 250 ha, buried the entire village of Hsiaolin in Kaohsiung County, resulting in 397 casualties, 53 people missing, and the destruction of over 100 houses (Lin et al., 2011; Tsou et al., 2011). To prevent such disasters, it is essential to map the areas that are susceptible to landslide for sustainable land-use management.

Landslide susceptibility can be defined as the probability of the occurrence of a landslide based on the relationship between the occurrence distribution and a set of predisposing factors, i.e. geo-environmental thematic variables in the area (Brabb, 1984; Guzzetti et al., 2005). Landslide susceptibility mapping involves handling, processing and interpreting a large amount of geographical data. Many studies have addressed landslide susceptibility mapping by various methods. Apart from the subjectivity of a direct (heuristic) approach completely based on field observations and an expert's priori knowledge, the remaining methods developed to detect the areas prone to landslide can be divided mainly into two categories: deterministic approach and statistical approach. The deterministic approach is based on the physical laws driving landslides and generally more applicable when the underground conditions are relatively homogeneous. The statistical approach is based on the relationships between the affecting factors and past and present landslide distribution (Van Westen et al., 2008). Statistical methods analyze the relation between all the factors affecting the landslide and are mainly focused on numerical methods such as linear or logistic regression (LR), artificial neural networks (ANN), frequency ratio (FR), and weight of evidence (WOE). In addition, landslide susceptibility assessment also involves the comparison of different statistical models (e.g., Lee and Pradhan, 2007, 2011; Akgun et al., 2008; Yilmaz, 2009, 2010a, b; Poudyal et al., 2010; Akgun, 2011; Pradhan and Lee, 2010a, c; Yalcin et al., 2011; Bui et al., 2012; Mohammady et al., 2012; Schicker and Moon, 2012; Xu et al., 2012; Ozdemir and Altural, 2013; Althuwaynee et al., 2014; Shahabi et al., 2014). To map the susceptibility to landslides, the WOE method calculates the weight for each factor affecting the landslide based on the presence or absence of landslides within



the study area (Van Westen et al., 2003; Lee and Choi, 2004; Kanungo et al., 2006; Mathew et al., 2007; Neuhäuser and Terhorst, 2007; Dahal et al., 2008a, b; Barbieri and Cambuli, 2009; Nandi and Shakoor, 2009; Regmi et al., 2010; Ozdemir, 2011; Mohammady et al., 2012; Schicker and Moon, 2012; Ozdemir and Altural, 2013). Conditional probability analysis is also a valuable tool in hazard zonation (Carrara et al., 1995), particularly when a few but relevant factors are available (Neuhäuser and Terhorst, 2007).

In the past, because of difficulties in obtaining detailed landslide data for each rainfall event, statistics-based landslide susceptibility evaluation models were based mainly on a long-term historical inventory of landslides induced by various rainfall events or earthquakes. Now, with highly developed remote sensing technology, multi-temporal satellite or aerial images have become an efficient way to map landslides after each event. Event-based multi-temporal landslide inventories are helpful for the understanding of recurrent landslide sites, and landslide occurrence criteria reflect the rainfall scale of storms and typhoons. Thus, the adoption of an event-based landslide inventory is beneficial in establishing an optimal landslide susceptibility evaluation model. To date, there is no comprehensive study involving the application of event-based multi-temporal landslide inventories to establish and validate a landslide susceptibility model. Lee et al. (2008) used an event-based landslide inventory to evaluate landslide susceptibility; however, only one typhoon event was used to establish the susceptibility model, and the suitability of the scale of the typhoon event adopted to establish the susceptibility model was not demonstrated. The present study evaluates susceptibility to landslides through a new landslide inventory based on typhoon events using Bayes' theorem based on the WOE method. We apply multi-temporal FORMOSAT-2 images to map four different rainfall scales of typhoon event-based new landslide inventories. To establish an optimal model we perform cross testing of four event-based landslide inventories, i.e. one model is calibrated based on one typhoon landslide inventory and validated by the other three typhoon landslide inventories. The area under curve (AUC) of the success rate curve (training sets) and the prediction rate curve (validation sets),

respectively, are applied to demonstrate the training and predictive performance of the susceptibility values obtained by the application of WOE (Van Westen et al., 2003; Poli and Sterlacchini, 2007). The dominant combination of factors related to landslide occurrence, and the most suitable typhoon scale to establish an optimal model are also discussed.

## 2 Study area

The Laonung River watershed of southern Taiwan with a total area of 1367 km$^2$ was selected as our study area (Fig. 1). The physiography ~~of the study area~~ is composed mainly ~~of~~ a series of approximately N–S to NE–SW trending mountain ranges. The elevation ~~of the study area~~ decreases westward and southward, from an elevation of 3941 m a.s.l. at the crest of Jade Mountain to 55 m a.s.l. at the foot of the mountain. The main river, the Lao-Nong River, flows SW and is one of the main tributaries of the Kaoping River.

For the convenience of discussion, the exposed rocks in the study area are roughly grouped according to their age and mechanical behavior into five stratigraphic units: slate, sandstone-shale, meta-sandstone, conglomerate and gravel, and sand (Fig. 1). The slope-angle distribution ~~of the study area,~~ calculated from a 5 m grid digital elevation model (DEM) falls in the range of 20–50° (78 % of the study area). The climate is a typical sub-tropical climate with a mean annual rainfall of about 2500 mm. Precipitation occurs mainly from May to September.

## 3 Materials and method

### 3.1 Event-based landslide inventories

Four typhoons (Table 1) that occurred in 2007–2009 and induced landslides were considered in the present study to ~~construct~~ the landslide susceptibility map. Landslides



of each typhoon in the study area were mapped from multi-spectral FORMOSAT-2 satellite images with 8 m pixel resolution taken before and after each typhoon event (Table 1). FORMOSAT-2 satellite images have been widely applied in identification of natural disasters (e.g., Lin et al., 2004, 2006, 2011; Liu et al., 2007). Mapping of the various types of landslides induced by each typhoon included landslides that are an extension of pre-existing landslides, as well as newly formed landslides.

On a FORMOSAT-2 multi-spectral image, shallow debris slides are the easiest type of slides to reliably detect because they strip off the vegetation cover and are thus readily discernable (Lin et al., 2011). Therefore, in this study we used mainly shallow debris slides. A landslide classification program based on Normalized Difference Vegetation Index (NDVI) distribution was used to identify bare land in images of the study area. Bare land in flat areas such as river beds was ruled out automatically by using a filter that deletes areas with a slope gradient less than 10°. Bare land caused by agriculture or urban development was excluded manually, leaving the landslide-induced bare land for the analysis. To prevent misinterpretation, only landslides with a projected area over nine pixels (representing areas larger than 576 m$^2$) were recognized. However, cases where the vegetation was stripped off due to deep-seated slides, such as the Hsiaolin landslide, and lateral erosion along the gully bed caused by debris flows were also included. All the mapped landslides in each typhoon event were transformed from vector format to raster format with 8 m pixel resolution. The mapped landslide inventories of four typhoons are shown in Fig. 2 and the landslide areas are summarized in Table 2, in which the landslide ratio is calculated as the total area of landslides per square km of the study area. The averaged cumulative rainfall brought by each typhoon listed in Table 2 was obtained from the Quantitative Precipitation Estimation and Segregation Using Multiple Sensors (QPESUMS) precipitation products of the Central Weather Bureau in Taiwan.

### 3.2 Affecting factors related to landslides

The geo-environmental features of an area affect the occurrence of landslides in different ways, and can be applied as affecting factors in the prediction of future landslides (Van Westen et al., 2008). The selection of affecting factors depends on the scale of the analysis, the characteristics of the study area, the landslide type, etc. (Glade et al., 2005). Nevertheless, there are no general guidelines for selecting these factors (Ayalew et al., 2005; Yalcin, 2008). In the present study, the affecting factors were selected among those most commonly used in the literature to evaluate landslide susceptibility; in particular, the results of field surveys and remote-sensing image interpretation suggest that the following eight parameters: geology (lithology), geomorphology (elevation, slope, aspect and landform), vegetation index, distance to geological structure, and distance to stream. To construct the landslide susceptibility model, the geomorphic parameters were directly extracted from a digital elevation model (DEM) with a resolution of 5 m pixel size created by the Ministry of Interior of Taiwan. These affecting factors are assumed constant over time except the vegetation index, which is extracted from the FORMOSAT-2 image taken before each typhoon event. Figure 3 shows the relevant factors like slope and aspect of the study area. The relation between the affecting factors and the landslides induced by the four typhoons is shown in Fig. 4, in which the landslide ratio was calculated as a ratio in percentage between the landslide area and the total area in each affecting factor class. The distribution of landslide ratios shows the relative importance of the different classes of affecting parameters to the landslide. Any area with a slope smaller than 5° and located in the main channel is treated as a stable area of the landslide and these cells are excluded in the categorization of the affecting factors.

Lithology is considered one of the main factors affecting landslide occurrence. By integrating the 1 : 50 000 geological map published by the Central Geology Survey of Taiwan, the variability of the lithologies in the study area is classified into five lithological groups: slate, sand-shale, meta-sandstone, conglomerate and gravel, and sand



(Fig. 1). The relation between the lithology and landslide inventories of the four typhoons shows that landslides occurred mainly in sandstone-shale and slate.

Elevation is a factor frequently utilized in landslide susceptibility assessment. The elevation in the study area varies from 55 to 3941 m; it was divided into thirteen heights at intervals of 250 m (Yalcin, 2008; Regmi et al., 2010; Tang et al., 2011). The relation between landslide distribution and elevation (Fig. 4) shows a significant variation among the four typhoons. In Typhoons Mitag, Sinlaku and Morakot, the elevation factor generally varies inversely to the landslide ratio while Typhoon Kalmagei shows an opposite trend. This is most likely due to the spatial variation of the wind and rainfall direction caused by the different tracks of the typhoons.

In previous studies of landslide susceptibility, slope was also considered as a major factor affecting slope stability (Anbalagan, 1992; Pachauri et al., 1998; Saha et al., 2002; Yalcin, 2008) because the driving force of mass movement increases with increasing slope (Guillard and Zezere, 2012). The slopes in the study area were divided into seven categories based on an interval of 10° (Van Westen et al., 2003; Dahal et al., 2008a, b, Regmi et al., 2010). The relation between landslides and slope angle (Fig. 4) shows that most of the landslides were observed for slopes > 30°. In Typhoon Morakot, many landslides occurred at slopes of 21–30° (nearly 6.7 % of the landslide ratio).

The aspect of the slope plays a role in controlling some microclimatic factors such as exposure to sunlight and windward (wet) or leeward (dry) conditions, rainfall intensity, soil moisture, and weathering, all of which control the material properties of the slope deposits (Dai et al., 2001; Cevik and Topal, 2003). The aspect of the study area was classified into eight classes (N, NE, E, SE, S, SW, W, and NW) with the addition of flat areas. Apart from the flat area, south-facing and SW-facing aspects dominate the aspect classes of the study area. The relation between aspect and landslide occurrences (Fig. 4) shows a similar trend for Typhoons Mitag, Sinlaku, and Morakot, where most of the landslides were observed in areas with south-facing slopes (SW, S, SE). However,

for Typhoon Kalmagei areas with north-facing slopes were dominant, probably due to the typhoon path that induced spatial variation in the rainfall.

Landform plays an important role in contributing to terrain instability, and can usually be analyzed by combing different types of curvatures such as plan curvature and profile curvature. The term curvature is theoretically defined as the rate of change of the slope gradient or aspect, usually in a particular direction (Wilson and Gallant, 2000). The curvature value can be evaluated by calculating the reciprocal value of the radius of the curvature in a particular direction and obtained directly from the derivatives of the topographical surface (Wilson and Gallant, 2000). The landform of the study area was classified into nine categories based on the method proposed by Dikau (1989). The relation between the landslide occurrence and landform (Fig. 4) shows that more landslides appeared in the concave valley landforms.

The vegetation index is also considered an influencing factor in landslide susceptibility assessment studies (Althuwaynee et al., 2012). NDVI was used in this study to reflect the vegetation density. In general, the value of NDVI ranged from −1 to 1; the higher the value of NDVI the denser of vegetation cover. The NDVI value was calculated by using the multi-spectrum information from the FORMOSAT-2 image based on the following formula.

$$\mathrm{NDVI} = \frac{\mathrm{NIR} - R}{\mathrm{NIR} + R} \quad (1)$$

where NIR is the reflectance in the near-infrared wave band and $R$ is the reflectance in the red wave band. The NDVI value in our study area was less than 0.8; therefore the NDVI was classified into four levels between 0–0.8 with a 0.2 interval, and a fifth level which included NDVI values less than 0. The relation between landslide occurrence and NDVI (Fig. 4) shows that most of the landslides were in areas with low NDVI values, especially NDVI < 0.

Geological structures such as faults, folds, and fractures usually play an important role in landslide formation. High susceptibility to landslides has been widely recorded at sites close to geological structure which not only affects the surface landform but



also contributes to soil permeability causing slope failure. The distance between the landslide and the geological structure in the study area was classified into ten lengths from 200 to 2000 m, at 200 m steps, with an additional eleventh category for distances greater than 2000 m (Lee and Choi, 2004; Vijith and Madhu, 2008). The relation between landslide occurrences and distance to geological structure (Fig. 4) shows that a large number of the landslides were observed in the area with a distance to geological structure ranging from 1400–2000 m.

The network of rivers and streams is another controlling parameter of landslide occurrence, as stream erosion may undercut the foot of the slopes as well as saturate their lower part (Dai et al., 2001; Saha et al., 2002; Cevik and Topal, 2003; Yalcin, 2008). The stream network was extracted by using the HYDRO tools of the ArcGIS software from the 5 m resolution DEM. The distance to the stream was then classified into nine lengths from 50 to 450 m, at 50 m steps with an additional tenth category for distances greater than 450 m. The "distance to stream" factor shows a significant inverse relation with landslide occurrences, the closer the site was to the stream, the more landslides were observed.

### 3.3 Weight of evidence

Weight-of-evidence (WOE) is one of the bivariate methods first applied to mineral exploration (Bonham-Carter et al., 1988). Subsequently, Van Westen et al. (2003) utilized the method for landslide susceptibility assessment. The theoretical background and its application in landslide susceptibility assessment are presented in many studies (see Introduction). The model is based on a log-linear form of Bayes' theorem, which calculates the weight for each affecting factor based on the combinational probabilities of its presence or absence with the presence or absence of a landslide within each map unit area (Bonham-Carter, 2002). The WOE method was documented mathematically by Van Westen et al. (2003) and Regmi et al. (2010) in detail. We calculated the weighted values for the classes of affecting factors related to landslides by using the following

equations (Regmi et al., 2010):

$$W^{+} = \ln\left(\frac{\frac{A_1}{A_1+A_2}}{\frac{A_3}{A_3+A_4}}\right) \quad (2)$$

$$W^{-} = \ln\left(\frac{\frac{A_2}{A_1+A_2}}{\frac{A_4}{A_3+A_4}}\right) \quad (3)$$

where $A_1$ is the number of landslide meshes present in a given factor class, $A_2$ is the number of landslide meshes not present in the given factor class, $A_3$ is the number of meshes in the given factor class in which no landslide meshes are present, and $A_4$ is the number of the meshes in which neither landslides nor the given factor are present. A positive weight ($W^+$) indicates the presence of the affecting factor in the landslide, and the magnitude of this weight is an indication of the positive correlation between the presence of the affecting factor and landslides. A negative weight ($W^-$) indicates an absence of the affecting factor, and its magnitude indicates negative correlation (Regmi et al., 2010). The difference between Eqs. (2) and (3) is defined as the weight contrast, $C$ ($C = W^+ - W^-$). A weight value of $C = 0$ indicates that the considered class of the affecting factor is not significant for the analysis. Positive or negative contrast indicates a positive or negative spatial correlation, respectively (Piacentini et al., 2012). The final landslide susceptibility index LSI is calculated by combining the probabilities associated with the different components of the model (Barbieri and Cambuli, 2009):

$$\mathrm{LSI} = \exp\left(\sum W^{+} + \ln(O_f)\right) \quad (4)$$

where $O_f = P_f/(1 - P_f)$ is the prior odds of a landslide in the study area, and $P_f = A_f/A_t$ where $A_f$ is the portion of the study area affected by landslides and $A_t$ is the total study area (Shicker and Moon, 2012).



## 4 Results and discussion

### 4.1 Testing for the predominant factors of landslides

The factors related to the occurrence of landslides are usually selected in the landslide susceptibility analysis. It is, however, worth discussing whether all the selected factors are required in the analysis. Previous studies have used effect analysis to identify factors or groups of factors that significantly influence landslide prediction (Van Westen et al., 2003; Dahal et al., 2008a, b). To do so, the factors are grouped directly, or in some cases certain factors are excluded before the weights are added. The predicted result is then compared to that obtained using all of the factors. Any obvious changes observed in the comparison would indicate the excluded or selected factors' significant impact on the prediction of landslides (Lee and Talib, 2005). In previous studies, effect analysis was mostly conducted by eliminating some of the factors or selecting certain factor combinations in order to observe the unselected factors and their effects on the results (Van Westen et al., 2003; Lee and Talib, 2005; Dahal et al., 2008a, b).

This study adopts an unconventional approach for the analysis. First, we select lithology and slope, the two most frequently used factors in previous studies, to be the primary factor combination for testing and analysis. Then, we enter additional factors and observe after each addition the changes to the AUC of the success rate curve. The process repeats itself and the factors are gradually accumulated until no more obvious changes in the AUC can be observed. The final test combination consists of eight factors. These factors were identified as the predominant factors of the landslides, having significant influences on the AUC of the success rate curve. Table 3 shows the test results for the predominant factor combinations of the typhoon events in the study. As the number of factors tested increases, the AUC also shows an increase. This highlights the increasing explanatory power of the factors. Using only four to five of the total eight factors for training, each typhoon event produces an AUC result similar to that of all eight factors, with a difference of less than 0.03. For example, the factor combination of lithology, slope, and NDVI reaches 90 % of the AUC of all the factors combined

for Typhoons Sinlaku, Mitag, and Kalmaegi; the combination of lithology, slope, and elevation reaches 90 % of the AUC for Typhoon Morakot. Therefore, lithology, slope, elevation, and ground vegetation are the predominant factors affecting a large number of landslides in the whole area. As for the other factors, aspect is affected by the spatial variation of the rainfall and wind during the typhoon or monsoon (i.e. whether the slope is facing windward or leeward).

From the perspective of statistics, effect analysis can indeed simplify the factor selection in the susceptibility analysis. In previous studies, effect analysis was conducted primarily in two ways: (1) a factor is excluded and the influence of the excluded factor on the result is assessed (Lee and Talib, 2005) and (2) factors are divided into categories of lithology, topography, and human cause; then, the categories are analyzed to assess the selected factors' influences on the results (Van Westen et al., 2003; Dahal et al., 2008a, b). The first method can identify the level of influence each factor has on the results, but it is only of statistical significance. Evaluating a factor as having a low level of influence does not mean it is not important in the susceptibility analysis (Lee and Talib, 2005) need more explanation. In addition, this method cannot find the optimum factor combination. The second method grouped factors based on lithology; however, the method cannot simplify factors effectively as it may overlook important ones in different categories. In our analysis we first select the fundamental factors of landslide according to the lithology of the study region. Then, we gradually increase the number of factors in the process of effect analysis. Our results show that although this method is more time-consuming compared to the previous two methods, it effectively simplifies the landslide factors without overlooking the important ones in the analysis process.

### 4.2 Landslide susceptibility mapping and validation

In this study, each of the four landslide susceptibility models is ~~created~~ based on an event-based landslide inventory of a single typhoon. The landslide inventories of three other typhoon events are used to validate the landslide susceptibility prediction. Table 4



shows the cross validation results of the events. Among the four typhoon events, Sinlaku exhibits the most favorable performance in establishing a susceptibility model, with the success rate of the curve's AUC reaching 0.933, followed by Mitag and Kalmaegi, with AUCs of 0.888 and 0.824, respectively. All three events show AUCs of over 80 %. The AUC of Morakot is 0.657, showing a less satisfactory performance. Table 4 shows a positive correlation between the validation result and the performance in establishing a susceptibility model. A higher AUC indicates a more favorable validation result. Generally among the four typhoons, the performance in establishing a susceptibility model and the validation result are directly proportional to the scale of the landsides caused by the typhoons. Better prediction results can be obtained by using the landslide susceptibility model created based on landslide inventories with lower landslide ratios (e.g. Mitag and Sinlaku). The susceptibility model established with the Typhoon Sinlaku event, for example, rendered satisfactory validation results in both Mitag and Kalmaegi. Mitag, in particular, showed the most favorable result, in which the AUC of the prediction rate curve reached 0.902. The model created based on Mitag also rendered an AUC of 0.889 in Sinlaku. The validation result of the model established based on Kalmaegi (with a new landslide rate of 1.021 %), on the other hand, only worked favorably for Mitag (0.712). As for Morakot, the performances for both the model and the validation were unsatisfactory. Thus, small-scale landslides tend to render better model performances because the relative weight between the landslide factors and landslide occurrence obtained using WOE often better reflects the critical threshold for the landslides. Morakot, the largest of the four typhoons, is the most severe typhoon that hit Taiwan in the past fifty years. The QPESUM data show a mean accumulated rainfall of 2323 mm in the study area (see Table 2). Rainfall of such scale far exceeds the critical rainfall threshold required for landslides to occur. As such, excessive landslides happened in the study area. In other words, when the landslide inventory of such a large-scale event is used to establish a model, the weight distribution among the landslide factors and landslide occurrence does not effectively distinguish areas that are susceptible to landslides from those that are not. Therefore, an inventory of a large-scale

landslide fails to accomplish the optimal performance in establishing a susceptibility model. By the same token, Morakot does not help identify the threshold of landslide occurrence because of the extensive landslide area. As a result, the validation result for Morakot is unfavorable.

Mitag and Kalmaegi show similar performances in establishing the susceptibility models; however, Mitag's validation result is clearly better than that of Kalmaegi. This is most likely caused by the slope aspect factor. The distribution of landslide ratios on the respective aspects for Kalmaegi is different from those of the other three typhoons (Fig. 4). Landslides that occurred during Mitag, Sinlaku, and Morakot show an obvious distribution on the south-facing aspects (SW, S, SE), while landslides caused by Kalmaegi concentrate around the north-facing aspects (NW, N, NE). As such, the distribution of weight contrast for Kalmaegi in terms of the aspects is opposite to those of the other three typhoons during the model training (Fig. 5). The northeast side of the study region is of a higher topography that gradually descends toward the southwest. Typhoons that rotate counterclockwise cause a greater number of landslides on the southern slope because it is the windward slope where rainfall is heavier, and this is true for Mitag, Sinlaku, and Morakot (Fig. 4). Despite the satisfactory training result of Kalmaegi, the validation result is unfavorable when we use different aspect factors from other events, as they affect the weights differently. Based on the above, we see that when a landslide susceptibility model is established based on a new landslide inventory of a single event, the selected inventory should be of a scale that is close to the landslide occurrence threshold and should reflect the most common spatial rainfall pattern in the study area for relatively ideal training and validation results.

Finally, based on the landslide inventory of Typhoon Sinlaku, which shows the best training and validation results, we created the landslide susceptibility map shown in Fig. 6. The susceptibility scale is based on the values of the horizontal axes of the prediction rate curves, with 0–0.1 = very high, 0.1–0.3 = high, 0.3–0.5 = moderate, 0.5–0.7 = low, and 0.7–1 = very low (Dahal et al., 2008a). The landslide ratios for each of the typhoons in the five susceptibility levels are listed in Table 5. Excluding Sinlaku, which



was used to establish the susceptibility model and the extreme event of Morakot, over 80 % of the actual landslide area of the other two typhoon events is covered by areas of very high and high susceptibility levels. For Mitag, 92.45 % of landslides occurred within the predicted landslide area, while 83.15 % of the Kalmaegi landslides were within the predicted range, indicating favorable prediction results of the landslide susceptibility map based on the landslide inventory of Typhoon Sinlaku.

Previous studies that used WOE to evaluate landslide susceptibility, for example, the study of an area of 500 $km^2$ in southwest Germany by Neuhäuser and Terhorst (2007), show prediction accuracy of 95 % for a single type of landslide. The study of newly formed debris flow in an area of 18.9 $km^2$ in the Lesser Himalayas of Nepal by Dahal et al. (2008a) achieved a prediction accuracy of 85.5 %. Dahal et al. (2008b) considered translational and flow slides in Moriyuki and Monnyu – two watershed areas in Japan, less than 4 $km^2$, to obtain a prediction accuracy of 80.7 and 77.6 %, respectively. A study of debris flows, debris slides, rock slides, and soil slides spanning 815 $km^2$ in Western Colorado, USA shows a prediction accuracy of 78 % (Regmi et al., 2010). Mohammady et al. (2012) considered rotational slides in a study area of 12 050 $km^2$ in Golestan Province, Iran and reached a prediction accuracy of 69 %. A study that used shallow landslides in an area of around 7500 $km^2$ in the south-eastern Alps, Italy obtained a prediction accuracy of 75 % (Piacentini et al., 2012). Ozdemir and Altural (2013), in a study region of 373 $km^2$ in the Sultan Mountain, SW Turkey, obtain 73.6 % predication accuracy. These studies indicate that the prediction accuracy is in a slightly negative correlation with the area of the study region. The larger the area, the greater the spatial difference among the topographic factors. This has an effect on the various types of landslides that occur. As a result, the training and validation results of landslide susceptibility models covering larger areas show unsatisfactory performances. Our study area spanned 1367 $km^2$, which is large compared with those in other relevant studies. The prediction accuracy of the landslide susceptibility map in this study reached 90.2 % in the best scenario. This supports the advantage of using a landslide

inventory of a single event to establish the landslide susceptibility model to predict landslide occurrence.

## 5 Conclusions

This study establishes single event-based landslide inventories for four different typhoons (i.e. Sinlaku, Mitag, Kalmaegi and Morakot) by using the multi-temporal Formosat-2 satellite imagery for the period 2007–2009. Using the weight of evidence (WOE) method, the inventories are adopted to analyze the relative weight between the landslide factors and landslide occurrences in the watershed of the Laonung River in southern Taiwan. Based on the results, a landslide susceptibility map is produced which can serve as a reference for planning and decision making regarding the use of the land. This study adopts eight factors for the landslide susceptibility analysis: lithology, elevation, slope, aspect, landform, NDVI, distance to lineation, and distance to stream. These factors are mapped in the study area based on a 5 m resolution DEM and satellite image data. We perform effect analysis as part of the assessment of the grouped factors to identify the dominant factors of landslide occurrence. Lithology and slope are selected as the primary factor combination for testing and analysis. The other factors are added one by one until the AUC of the success rate curve does not show any further obvious changes. The test results indicate that lithology, slope, elevation, and ground vegetation are the dominant factors affecting most landslide incidents in the study area. These four factors can help achieve 90 % of the AUC of the all-factor success rate curve. As the number of selected factors increases in the process, the success rate curve gradually converges to a point where the result generally resembles that of the all-factor analysis. This means that there is no need for a large number of factors to achieve a reliable landslide susceptibility analysis. Fewer factors can provide results similar to those utilizing a large number of factors.

This study uses a new landslide inventory of a single event to establish a landslide susceptibility model. Each model uses three other inventories to validate the prediction



of landslide susceptibility. Cross validation results show that the performance of the susceptibility model and the validation result are directly proportional to the scale of the landsides caused by the typhoons. Using inventories with lower landslide ratios to build the landslide susceptibility models leads to more favorable landslide prediction results. For example, the AUCs of the success rate curves for Sinlaku and Mitag were 0.933 and 0.888, respectively. The model established based on Sinlaku shows satisfactory validation results in Mitag and Kalmaegi. Mitag has the best result, with the AUC of the prediction rate curve reaching 0.902. The model established using Mitag, on the other hand, also provides an AUC of 0.889 in Sinlaku. Mitag's performance in establishing a susceptibility model is similar to that of Kalmaegi, although Mitag's validation result is clearly better than the result of Kalmaegi. This difference is caused by the slope aspect factor. Landslides caused by Mitag, Sinlaku, and Morakot concentrated on the south-facing aspects (SW, S, SE), while those caused by Kalmaegi occurred around the north-facing aspects (NW, N, NE). Therefore, the distribution of weight contrast for Kalmaegi in terms of individual aspects is opposite to those of the other three typhoons.

Landslides of a smaller scale tend to show a better performance in establishing a susceptibility model. This is because the relative weight between the landslide factors and landslide occurrences in the WOE analysis can often better reflect the threshold for landslides to occur. The extensive, heavy rainfall brought by Morakot far exceeded the critical threshold required for landslides to occur. When a model is created with such a large-scale event, the relative weights between the individual landslide factors and landslide occurrences fail to distinguish areas susceptible to landslides from those that are not. The performances are thus unsatisfactory in establishing a susceptibility model and validating the events.

Last but not least, Typhoon Sinlaku, which demonstrated the best training and validation results in the study, was selected to produce the landslide susceptibility map. Excluding the extreme event of Morakot, more than 80 % of the actual landslide area resulting from Typhoons Mitag and Kalmaegi is covered in our susceptibility map by areas denoted as having very high and high susceptibility to landslides. This indicates

that using the landslide inventory based on the single event of Sinlaku to create the map renders good prediction results on landslide occurrence. Previous studies that use WOE for landslide susceptibility analysis suggest that the prediction accuracy and the area of the study region are inversely related. The larger the study area, the greater the spatial differences among topographic factors such as lithology, elevation, slope, aspect, and landform. The types of landslides that occur are thus more diverse and complex. As a result, the landslide susceptibility model is less effective. Our study area is considered large compared to those in previous studies. The prediction accuracy of the landslide susceptibility map created by this study reached 90.2 %, validating the advantage of a landslide susceptibility model established by using a landslide inventory based on a single event. According to the results of this study, when a new landslide inventory of a single event is used to create a landslide susceptibility model, the inventory selected should be of a scale that is close to the landslide occurrence threshold, and is able to reflect the most common spatial rainfall pattern in the study area for best prediction results.

## References


Akgun, A.: A comparison of landslide susceptibility maps produced by logistic regression, multicriteria decision, and likelihood ratio methods: a case study at İzmir, Turkey, Landslides, 9, 93–106, 2011.

Akgun, A., Dag, S., and Bulut, F.: Landslide susceptibility mapping for a landslideprone area (Findikli, NE of Turkey) by likelihood frequency ratio and weighted linear combination models, Environ. Geol., 54, 1127–1143, 2008.

Althuwaynee, O. F., Pradhan, B., and Lee, S.: Application of an evidential belief function model in landslide susceptibility mapping, Comput. Geosci., 44, 120–135, 2012.

Althuwaynee, O. F., Pradhan, B., Park, H. J., and Lee, J. H.: A novel ensemble bivariate statistical evidential belief function with knowledge-based analytical hierarchy process and multivariate statistical logistic regression for landslide susceptibility mapping, Catena, 114, 21–36, 2014.





Anbalagan, D.: Landslide hazard evaluation and zonation mapping in mountainous terrain, Eng. Geol., 32, 269–277, 1992.

Ayalew, L., Yamagishi, H., Marui, H., and Kanno, T.: Landslides in Sado Island of Japan Part II. GIS-based susceptibility mapping with comparisons of results from two methods and verifications, Eng. Geol., 81, 432–445, 2005.

Barbieri, G. and Cambuli, P.: The weight of evidence statistical method in landslide susceptibility mapping of the Rio Pardu Valley (Sardinia, Italy), 18th World IMACS/MODSIM Congress, Cairns, Australia, 13–17 July, 2009, 2658–2664, 2009.

Bonham-Carter, G. F.: Geographic information systems for geoscientists: modelling with GIS, in: Computer Methods in the Geosciences, edited by: Merriam, D. F., 13, Pergamon/Elsevier, New York, 302–334, 2002.

Bonham-Carter, G. F., Agterberg, F. P., and Wright, D. F.: Weights of evidence modelling: a new approach to mapping mineral potential, Stat. Appl. Earth Sci., 89, 171–183, 1988.

Brabb, E. E.: Innovative approaches to landslide hazard and risk mapping, Proceedings of the Fourth International Symposium on Landslides, Canadian Geotechnical Society, Toronto, Canada, 16–21 September, 1984, 1, 307–324, 1984.

Brabb, E. E. and Harrod, B. L. (Eds.): Landslides: Extent and Economic Significance, Balkema Publisher, Rotterdam, 1989.

Bui, D. T., Pradhan, B., Lofman, O., Revhaug, I., and Dick, O. B.: Landslide susceptibility assessment in the Hoa Binh province of Vietnam: a comparison of the Levenberg–Marquardt and Bayesian regularized neural networks, Geomorphology, 171–172, 12–29, 2012.

Carrara, A., Cardinali, A., Guzzetti, F., and Reichenbach, P.: GIS based techniques for mapping landslide hazard, in: Geographical Information Systems in Assessing Natural Hazards, edited by: Carrara, A. and Guzzetti, F., Kluwer Academic Publications, Dordrecht, The Netherlands, 135–176, 1995.

Cendrero, A. and Dramis, F.: The contribution of landslides to landscape evolution in Europe, Geomorphology, 15, 191–211, 1996.

Çevik, E. and Topal, T.: GIS-based landslide susceptibility mapping for a problematic segment of the natural gas pipeline, Hendek (Turkey), Environ. Geol., 44, 949–962, 2003.

Dahal, R. K., Hasegawa, S., Nonomura, A., Yamanaka, M., Dhakal, S., and Paudyal, P.: Predictive modelling of rainfall-induced landslide hazard in the Lesser Himalaya of Nepal based on weights-of-evidence, Geomorphology, 102, 496–510, 2008a.

Dahal, R. K., Hasegawa, S., Nonomura, A., Yamanaka, M., Masuda, T., and Nishino, K.: GIS-based weights-of-evidence modelling of rainfall-induced landslides in small catchments for landslide susceptibility mapping, Environ. Geol., 54, 311–324, 2008b.

Dai, F. C., Lee, C. F., and Xu, Z. W.: Assessment of landslide susceptibility on the natural terrain of Lantau Island, Hong Kong, Environ. Geol., 40, 381–391, 2001.

Dikau, R.: The application of a digital relief model to landform analysis in geomorphology, in: Three Dimensional Applications in Geographic Informations Systems, edited by: Raper, J., Taylor and Francis, London, 51–77, 1989.

Glade, T., Anderson, M., and Crozier, M. J. (Eds.): Landslide Hazard and Risk, Wiley, New York, 2005.

Guzzetti, F., Carrara, A., Cardinali, M., and Reichenbach, P.: Landslide hazard evaluation: an aid to a sustainable development, Geomorphology, 31, 181–216, 1999.

Guzzetti, P., Reichenbach, M., Cardinali, M., Galli, F., and Ardizzone, F.: Landslide hazard assessment in the Staffora basin, northern Italian Apennines, Geomorphology, 72, 272–299, 2005.

Guillard, C. and Zezere, J.: Landslide susceptibility assessment and validation in the framework of municipal planning in portugal: the case of Loures Municipality, Environ. Manage., 50, 721–735, 2012.

Kanungo, D. P., Arora, M. K., Sarkar, S., and Gupta, R. P.: A comparative study of conventional, ANN black box, fuzzy and combined neural and fuzzy weighting procedures for landslide susceptibility zonation in Darjeeling Himalayas, Eng. Geol., 85, 347–366, 2006.

Lee, C. T., Huang, C. C., Lee, J. F., Pan, K. L., Lin, M. L., and Dong, J. J.: Statistical approach to storm event-induced landslides susceptibility, Nat. Hazards Earth Syst. Sci., 8, 941–960, doi:10.5194/nhess-8-941-2008, 2008.

Lee, S. and Choi, J.: Landslide susceptibility mapping using GIS and the weight-of-evidence model, Int. J. Geogr. Inf. Sci., 18, 789–814, 2004.

Lee, S. and Pradhan, B.: Landslide hazard mapping at Selangor, Malaysia using frequency ratio and logistic regression models, Landslides, 4, 33–41, 2007.

Lee, S. and Talib, J. A.: Probabilistic landslide susceptibility and factor effect analysis, Environ. Geol., 47, 982–990, 2005.

Lin, C. W., Shieh, C. J., Yuan, B. D., Shieh, Y. C., Huang, M. L., and Lee, S. Y.: Impact of Chi-Chi earthquake on the occurrence of landslides and debris flows: example from the Chenyulan River watershed, Nantou, Taiwan, Eng. Geol., 71, 49–61, 2004.



Lin, C. W., Liu, S. H., Lee, S. Y., and Liu, C. C.: Impacts of the Chi-Chi earthquake on subsequent rainfall-induced landslides in central Taiwan, Eng. Geol., 86, 87–101, 2006.

Lin, C. W., Chang, W. S., Liu, S. H., Tsai, T. T., Lee, S. P., Tsang, Y. C., Shieh, C. L., and Tseng, C. M.: Landslides triggered by the 7 August 2009 Typhoon Morakot in Southern Taiwan, Eng. Geol., 123, 3–12, 2011.

Lin, C. W., Tseng, C. M., Tseng, Y. H., Fei, L. Y., Hsieh, Y. C., and Tarolli, P.: Recognition of large scale deep-seated landslides in forest areas of Taiwan using high resolution topography, J. Asian Earth Sci., 62, 389–400, 2013.

Liu, C. C., Liu, J. G., Lin, C. W., Wu, A. M., Liu, S. H., and Shieh, C. L.: Image processing of FORMOSAT-2 data for monitoring South Asia tsunami, Int. J. Remote Sens., 28, 3093–3111, 2007.

Mathew, J., Jha, V. K., and Rawat, G. S.: Application of binary logistic regression analysis and its validation for landslide susceptibility mapping in part of Garhwal Himalaya, India, Int. J. Remote Sens., 28, 2257–2275, 2007.

Mohammady, M., Pourghasemi, H. R., and Pradhan, B.: Landslide susceptibility mapping at Golestan Province, Iran: a comparison between frequency ratio, Dempster–Shafer, and weights-of-evidence models, J. Asian Earth Sci., 61, 221–236, 2012.

Nandi, A. and Shakoor, A.: A GIS-based landslide susceptibility evaluation using bivariate and multivariate statistical analyses, Eng. Geol., 110, 11–20, 2009.

Neuhäuser, B. and Terhorst, B.: Landslide susceptibility assessment using weights-of-evidence applied to a study area at the Jurassic escarpment (SW Germany), Geomorphology, 86, 12–24, 2007.

Ozdemir, A.: Landslide susceptibility mapping using Bayesian approach in the Sultan Mountains (Aks_ehir, Turkey), Nat. Hazards, 59, 1573–1607, 2011.

Ozdemir, A. and Altural, T.: A comparative study of frequency ratio, weights of evidence and logistic regression methods for landslide susceptibility mapping: Sultan Mountains, SW Turkey, J. Asian Earth Sci., 64, 180–197, 2013.

Pachauri, A. K., Gupta, P. V., and Chander, R.: Landslide zoning in a part of the Garhwal Himalayas, Environ. Geol., 36, 325–334, 1998.

Piacentini, D., Troiani, F., Soldati, M., Notarnicola, C., Savelli, D., Schneiderbauer, S., and Strada, C.: Statistical analysis for assessing shallow-landslide susceptibility in South Tyrol (south-eastern Alps, Italy), Geomorphology, 151–152, 196–206, 2012.

Poudyal, C. P., Chang, C., Oh, H. J., and Lee, S.: Landslide susceptibility maps comparing frequency ratio and artificial neural networks: a case study from the Nepal Himalaya, Environ. Earth Sci., 61, 1049–1064, 2010.
Poli, S. and Sterlacchini, S.: Landslide representation strategies in susceptibility studies using weights-of-evidence modeling technique, Nat. Resour. Res., 16, 121–134, 2007.
Pradhan, B.: Manifestation of an advanced fuzzy logic model coupled with geo-information techniques to landslide susceptibility mapping and their comparison with logistic regression modelling, Environ. Ecol. Stat., 18, 471–493, 2011.
Pradhan, B. and Lee, S.: Delineation of landslide hazard areas on Penang Island, Malaysia, by using frequency ratio, logistic regression, and artificial neural network models, Environ. Earth Sci., 60, 1037–1054, 2010a.
Pradhan, B. and Lee, S.: Regional landslide susceptibility analysis using back-propagation neural network model at Cameron Highland, Malaysia, Landslides, 7, 13–30, 2010b.
Pradhan, B. and Lee, S.: Landslide susceptibility assessment and factor effect analysis: back-propagation artificial neural networks and their comparison with frequency ratio and bivariate logistic regression modelling, Environ. Modell. Softw., 25, 747–759, 2010c.
Regmi, N. R., Giardino, J. R., and Vitek, J. D.: Modeling susceptibility to landslides using the weight of evidence approach: Western Colorado, USA, Geomorphology, 115, 172–187, 2010.
Saha, A. K., Gupta, R. P., and Arora, M. K.: GIS-based landslide hazard zonation in the Bhagirathi (Ganga) valley, Himalayas, Int. J. Remote Sens., 23, 357–369, 2002.
Schicker, R. and Moon, V.: Comparison of bivariate and multivariate statistical approaches in landslide susceptibility mapping at a regional scale, Geomorphology, 162, 40–57, 2012.
Shahabi, H., Khezri, S., Ahmad, B. B., and Hashim, M.: Landslide susceptibility mapping at central Zab basin, Iran: a comparison between analytical hierarchy process, frequency ratio and logistic regression models, Catena, 115, 55–70, 2014.
Tang, C., Zhu, J., Qi, X., and Ding, J.: Landslides induced by the Wenchuan earthquake and the subsequent strong rainfall event: a case study in the Beichuan area of China, Eng. Geol., 122, 22–33, 2011.
Tsou, C. Y., Feng, Z. Y., and Chigira, M.: Catastrophic landslide induced by Typhoon Morakot, Shiaolin, Taiwan, Geomorphology, 127, 166–178, 2011.





Tseng, C. M., Lin, C. W., Stark, C. P., Liu, J. K., Fei, L. Y., and Hsieh, Y. C.: Application of a multi-temporal, LiDAR-derived, digital terrain model in a landslide-volume estimation, Earth Surf. Proc. Land., 38, 1587–1601, 2013.
Van Westen, C. J., Rengers, N., and Soeters, R.: Use of geomorphological information in indirect landslide assessment, Nat. Hazards, 30, 399–419, 2003.
Van Westen, C. J., Castellanos, E., and Kuriakose, S. L.: Spatial data for landslide susceptibility, hazard, and vulnerability assessment: an overview, Eng. Geol., 102, 112–131, 2008.
Vijith, H. and Madhu, G.: Estimating potential landslide sites of an upland sub-watershed in Western Ghat's of Kerala (India) through frequency ratio and GIS, Environ. Geol., 55, 1397–1405, 2008.
Wilson, J. P. and Gallant, J. G.: Terrain Analysis Principles and Applications, John Wiley and Sons, Inc., New York, 2000.
Xu, C., Xu, X., Dai, F., Xiao, J., Tan, X., and Yuan, R.: Landslide hazard mapping using GIS and weight of evidence model in Qingshui River watershed of 2008 Wenchuan earthquake struck region, J. Earth Sci., 23, 97–120, 2012.
Yalcin, A.: GIS-based landslide susceptibility mapping using analytical hierarchy process and bivariate statistics in Ardesen (Turkey): comparisons of results and confirmations, Catena, 72, 1–12, 2008.
Yalcin, A., Reis, S., Aydinoglu, A. C., and Yomralioglu, T.: A GIS-based comparative study of frequency ratio, analytical hierarchy process, bivariate statistics and logistics regression methods for landslide susceptibility mapping in Trabzon, NE Turkey, Catena, 85, 274–287, 2011.
Yilmaz, I.: Landslide susceptibility mapping using frequency ratio, logistic regression, artificial neural networks and their comparison: a case study from Kat landslides (Tokat-Turkey), Comput. Geosci., 35, 1125–1138, 2009.
Yilmaz, I.: Comparison of landslide susceptibility mapping methodologies for Koyulhisar, Turkey: conditional probability, logistic regression, artificial neural networks, and support vector machine, Environ. Earth Sci., 61, 821–836, 2010a.
Yilmaz, I.: The effect of the sampling strategies on the landslide susceptibility mapping by conditional probability and artificial neural networks, Environ. Earth Sci., 60, 505–519, 2010b.

**Table 1.** FORMOSAT-2 images used to map the event-based landslide inventories in this study.

| Typhoon event | Date | Date of images taken (pre//post of typhoon) |
|---|---|---|
| Mitag | 24–27 Nov 2007 | 26 Oct 2007, 20 Nov 2007 // 21 Dec 2007, 17 Feb 2008 |
| Kalmaegi | 16–18 Jul 2008 | 21 Dec 2007, 17 Feb 2008 // 23 Jul 2008, 24 Aug 2008 |
| Sinlaku | 11–16 Sep 2008 | 23 Jul 2008, 24 Aug 2008 // 21 Dec 2008, 14 Jan 2009 |
| Morakot | 5–10 Aug 2009 | 21 Dec 2008, 14 Jan 2009 // 17 Aug 2009, 21 Aug 2009 |





**Table 2.** Landslide data interpreted from FORMOSAT-2 images for the four typhoon events.

| Typhoon event | Averaged rainfall accumulated (mm) | Landslide area (ha) | Landslide ratio (%) |
|---|---|---|---|
| Mitag | 60 | 440 | 0.322 |
| Kalmaegi | 712 | 1452 | 1.062 |
| Sinlaku | 774 | 593 | 0.434 |
| Morakot | 2323 | 8946 | 6.544 |

**Table 3a.** Test results for various combinations of dominant factors of landslides. Typhoon Mitag and Sinlaku.

| No. | Combination of factors | Training AUC Mitag | Sinlaku |
|---|---|---|---|
| A1 | Sa + Lc | 0.561 | 0.606 |
| A2 | Sa + Lc + As | 0.708 | 0.786 |
| A3 | Sa + Lc + Lf | 0.567 | 0.618 |
| A4 | Sa + Lc + El | 0.682 | 0.697 |
| A5 | Sa + Lc + Dl | 0.596 | 0.633 |
| A6 | Sa + Lc + Ds | 0.634 | 0.681 |
| A7 | Sa + Lc + Nv | 0.799 | 0.857 |
| A8 | Sa + Lc + Nv + As | 0.870 | 0.912 |
| A9 | Sa + Lc + Nv + Lf | 0.801 | 0.859 |
| A10 | Sa + Lc + Nv + El | 0.824 | 0.891 |
| A11 | Sa + Lc + Nv + Dl | 0.810 | 0.865 |
| A12 | Sa + Lc + Nv + Ds | 0.817 | 0.872 |
| A13 | Sa + Lc + Nv + As + Lf | 0.870 | 0.913 |
| A14 | Sa + Lc + Nv + As + El | 0.882 | 0.931 |
| A15 | Sa + Lc + Nv + As + Dl | 0.874 | 0.915 |
| A16 | Sa + Lc + Nv + As + Ds | 0.879 | 0.920 |
| A17 | Total eight factors | 0.888 | 0.933 |

Sa: slope angle; Lc: lithology condition; As: aspect; Lf: landform; El: elevation; Dl: distance to lineation; Ds: distance to stream; Nv: NDVI.





**Table 3b.** Test results for various combinations of dominant factors of landslides. Typhoon Kalmaegi.

| No. | Combination of factors | Training AUC Kalmaegi |
|---|---|---|
| B1 | Sa + Lc | 0.616 |
| B2 | Sa + Lc + As | 0.626 |
| B3 | Sa + Lc + Lf | 0.628 |
| B4 | Sa + Lc + El | 0.643 |
| B5 | Sa + Lc + Dl | 0.624 |
| B6 | Sa + Lc + Ds | 0.649 |
| B7 | Sa + Lc + Nv | 0.820 |
| B8 | Sa + Lc + Nv + As | 0.791 |
| B9 | Sa + Lc + Nv + Lf | 0.823 |
| B10 | Sa + Lc + Nv + El | 0.823 |
| B11 | Sa + Lc + Nv + Dl | 0.821 |
| B12 | Sa + Lc + Nv + Ds | 0.826 |
| B13 | Sa + Lc + Nv + Ds + As | 0.815 |
| B14 | Sa + Lc + Nv + Ds + Lf | 0.829 |
| B15 | Sa + Lc + Nv + Ds + El | 0.831 |
| B16 | Sa + Lc + Nv + Ds + Dl | 0.828 |
| B17 | Total eight factors | 0.824 |

**Table 3c.** Test results for various combinations of dominant factors of landslides. Typhoon Morakot.

| No. | Combination of factors | Training AUC Morakot |
|---|---|---|
| C1 | Sa + Lc | 0.556 |
| C2 | Sa + Lc + As | 0.579 |
| C3 | Sa + Lc + Lf | 0.568 |
| C4 | Sa + Lc + Nv | 0.576 |
| C5 | Sa + Lc + Dl | 0.568 |
| C6 | Sa + Lc + Ds | 0.582 |
| C7 | Sa + Lc + El | 0.624 |
| C8 | Sa + Lc + El + As | 0.635 |
| C9 | Sa + Lc + El + Lf | 0.626 |
| C10 | Sa + Lc + El + Dl | 0.626 |
| C11 | Sa + Lc + El + Ds | 0.633 |
| C12 | Sa + Lc + El + Nv | 0.636 |
| C13 | Sa + Lc + El + Nv + As | 0.646 |
| C14 | Sa + Lc + El + Nv + Lf | 0.639 |
| C15 | Sa + Lc + El + Nv + Dl | 0.637 |
| C16 | Sa + Lc + El + Nv + Ds | 0.642 |
| C17 | Total eight factors | 0.657 |





**Table 4.** Validation results of landslide susceptibility model established by each typhoon.

| Events | LR (%) | AUC (Training) | AUC (Validation) | | | |
|---|---|---|---|---|---|---|
| | | | Mitag | Kalmaegi | Sinlaku | Morakot |
| Mitag | 0.303 | 0.888 | – | 0.796 | 0.889 | 0.603 |
| Kalmaegi | 1.021 | 0.824 | 0.712 | – | 0.636 | 0.512 |
| Sinlaku | 0.482 | 0.933 | 0.902 | 0.844 | – | 0.648 |
| Morakot | 7.218 | 0.657 | 0.656 | 0.582 | 0.737 | – |

**Table 5.** Distribution of landslides induced by the four typhoons for each susceptibility level.

| Typhoon events | Very high (0–10 %) | High (10–30 %) | Moderate (30–50 %) | Low (50–70 %) | Very low (70–100 %) |
|---|---|---|---|---|---|
| Mitag | 73.47 % | 18.98 % | 4.26 % | 2.33 % | 0.96 % |
| Kalmeagi | 50.04 % | 33.11 % | 12.09 % | 4.34 % | 0.42 % |
| Sinlaku | 80.49 % | 15.61 % | 3.13 % | 0.57 % | 0.21 % |
| Morakot | 19.38 % | 30.50 % | 22.17 % | 14.71 % | 13.24 % |





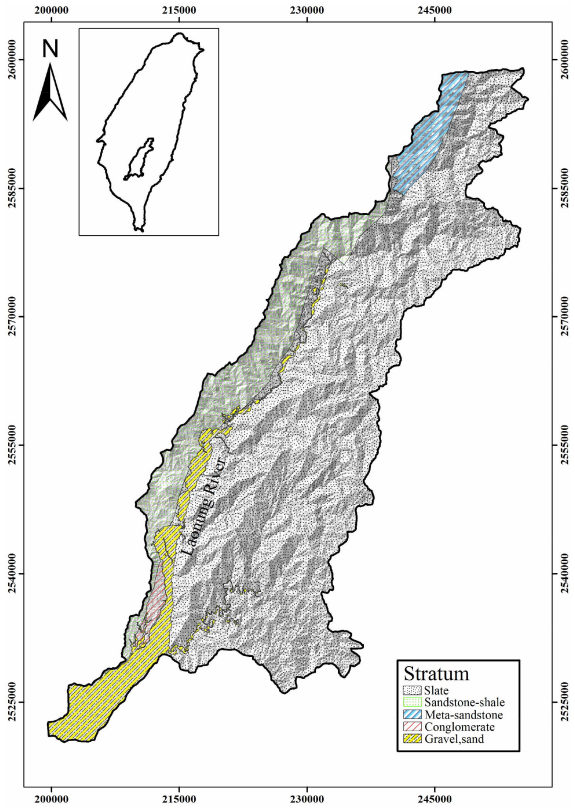


**Figure 1.** Geological map of the study area. The bold black line shows the study area.

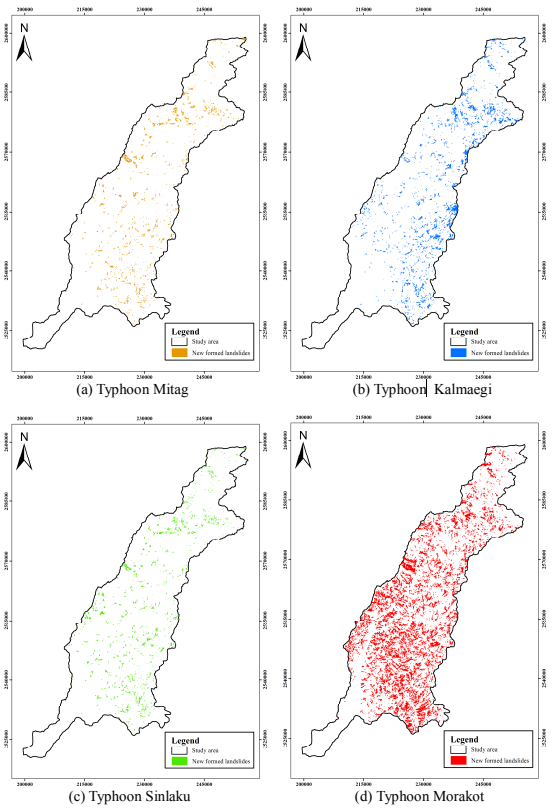


**Figure 2.** Event-based landslide inventories interpreted by multi-temporal FORMOSAT-2 satellite images.





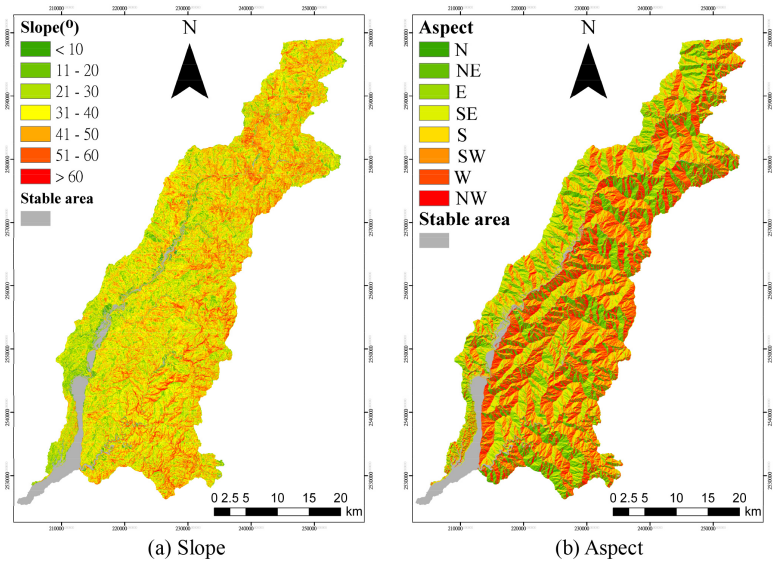


**Figure 3.** Spatial distribution of factors affecting landslide susceptibility assessment: **(a)** slope, **(b)** aspect.

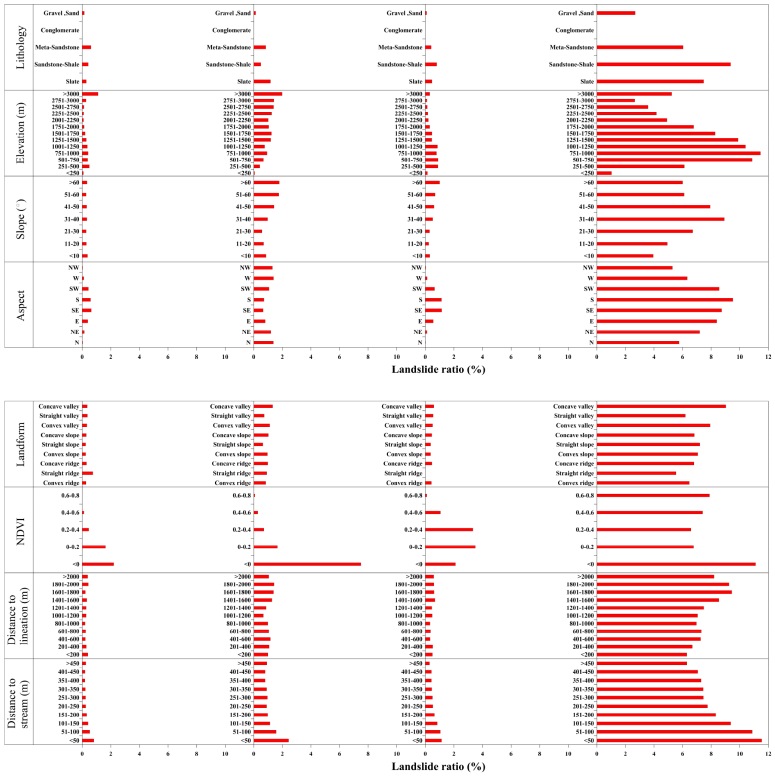


(a) Typhoon Mitag (b) Typhoon Kalmagei (c) Typhoon Sinlaku (d) Typhoon Morakot

**Figure 4.** Landslide ratios for the eight landslide affecting factors of the four typhoon events.



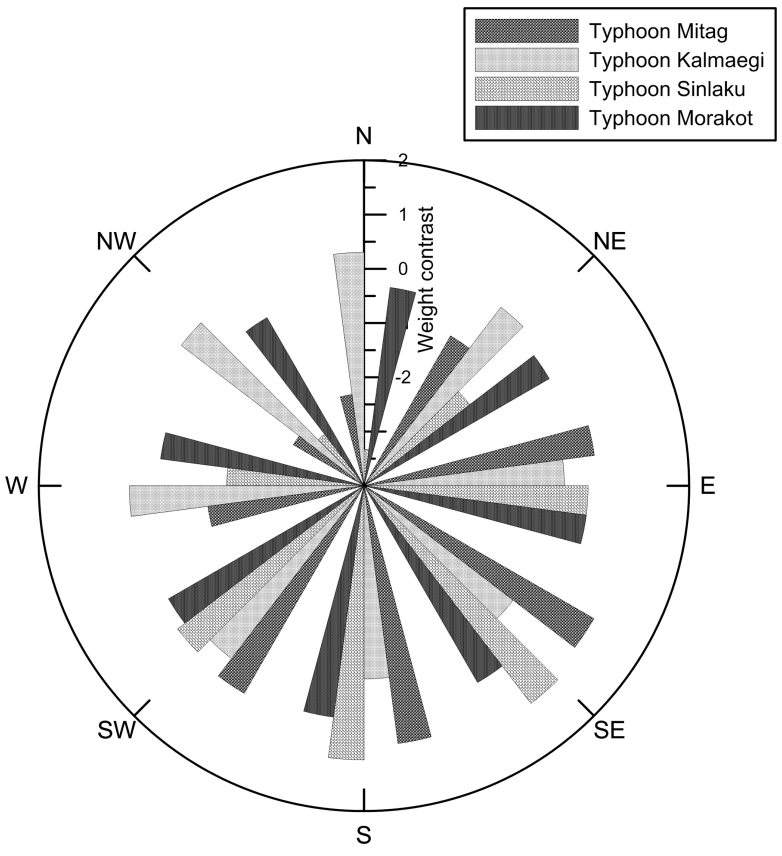


**Figure 5.** Variation of weight contrast at different slope aspect directions.

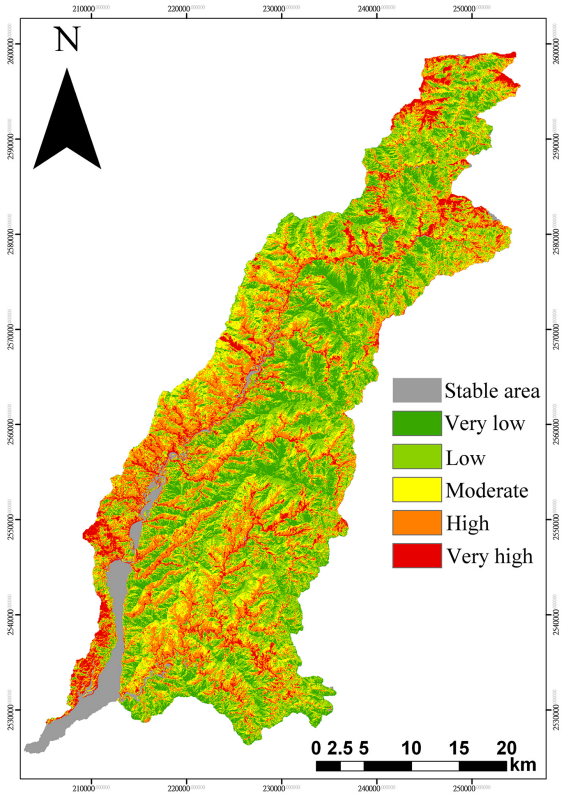


**Figure 6.** Landslide susceptibility map of the study area.